# PV Frontogenesis and Upper-Tropospheric Fronts

H. C. DAVIES

*Institute for Atmospheric Science, Zurich, Switzerland*

A. M. ROSSA

*Swiss Meteorological Institute, Zurich, Switzerland*

(Manuscript received 21 March 1997, in final form 15 September 1997)

ABSTRACT

Upper-tropospheric fronts and frontogenesis are viewed from a potental vorticity (PV) perspective. The rudiments of this approach are to regard such a front as a zone of strong PV gradient on isentropic surfaces, and to treat the accompanying frontogenesis as the process whereby this gradient is enhanced on tropopause-transcending isentropic surfaces. A case study suggests that this concept of PV frontogenesis provides a concise dynamically based definition of upper-level frontal zones, and a compact and transparent approach for diagnosing the frontogenesis. The concept provides fresh insight on the dynamics of the upper-level fronts, and has the potential to shed light on related phenomena and processes.

## 1. Introduction

Upper-tropospheric fronts are systems characterized by enhanced values of baroclinicity, lateral shear, and vertical stratification. They are elongated systems aligned along the flow, and in the across-front direction they distort and transect the tropopause. Figure 1 depicts a section across such a front derived from the routine operational analysis fields of the ECMWF. It reveals the forementioned characteristics with a sharp tropopause break collocated with a jet, and also slanting zones of enhanced baroclinicity and stratification located below, and to a lesser degree above, the jet.

The occurrence and dynamics of such fronts is of intrinsic theoretical interest as an example of the formation of elongated coherent structures with tight gradients in geophysical fluid systems. They are also of considerable practical importance in that they can influence the maintenance and/or dissolution of the tropopause itself, the form and extent of stratosphere–troposphere exchange, and the development of surface weather patterns.

Here upper-troposphere fronts are examined from a potential vorticity (PV) perspective (Hoskins et al. 1985). The objectives of the study relate to the following set of questions. Is the adoption of such a perspective physically meaningful? What do fronts look like within this framework? What additional insight, if any, accrues from pursuing this alternative approach? To address these questions we consider the rudiments of the PV perspective of fronts (section 2), present a heuristic case study of a PV frontogenesis event (section 3), and comment upon conventional and other approaches (section 4).

*Corresponding author's address:* H. C. Davies, Institute for Atmospheric Science, ETH Hönggerberg, CH-8093 Zurich, Switzerland.
E-mail: davies@atmos.umnw.ethz.ch

## 2. Rudiments of the PV perspective

The kernel of the present approach is (a) to identify upper-level fronts as elongated zones of strong PV gradient on isentropic surfaces (i.e., $\nabla_\theta$PV), and (b) to view the accompanying frontogenesis as the process whereby this gradient is enhanced on tropopause-transcending isentropic surfaces. We consider these two concepts in turn.

### *a. PV fronts*

The concept of a PV front is lent some credence by inspection of Fig. 1. There are indications of a spatially confined and strong gradient of $\nabla_\theta$PV in the vicinity of the jet. A more transparent depiction of this feature is provided in Fig. 2. It displays the PV distribution and the field of $\nabla_\theta$PV for the same cross section as the previous figure but now with $\theta$ as the vertical coordinate. In this coordinate system the concept of a PV front would imply that the field of $\nabla_\theta$PV should exhibit a highly localized maximum. The figure indicates that, at least for the displayed event, there is a unique and spatially well-defined PV front.

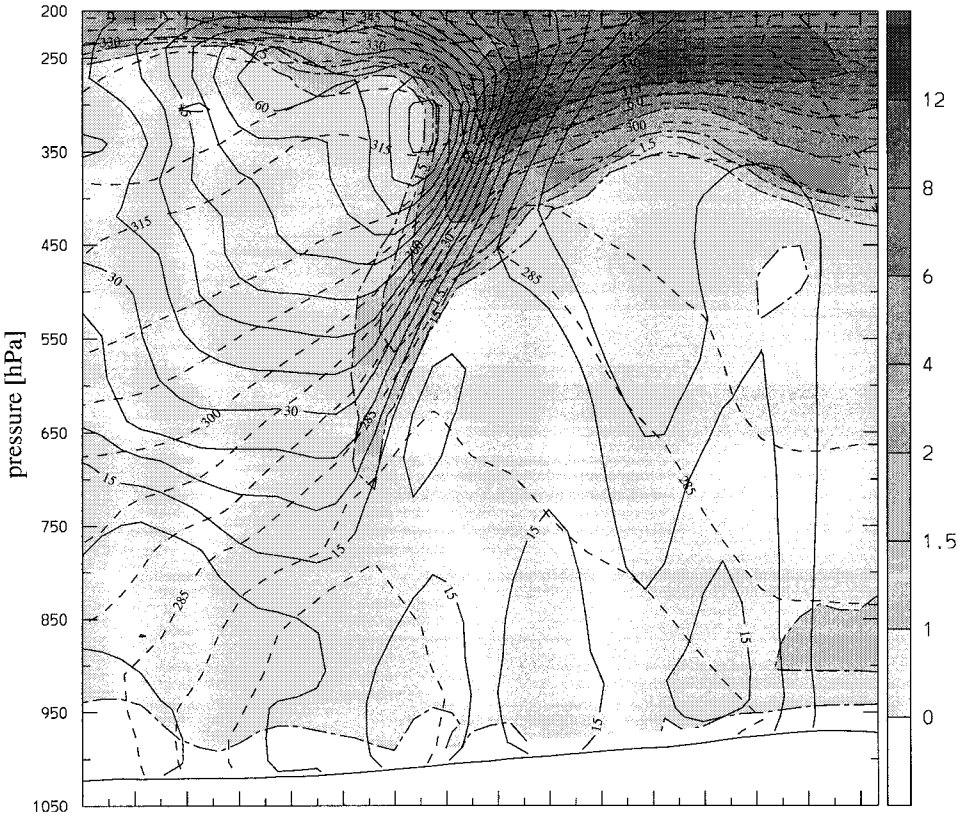


FIG. 1. A section across a mid-Atlantic front at 1200 UTC 22 November 1992 derived from ECMWF operational analyses. The location of the section is indicated in Fig. 7d, and extends from 40°N, 55°W on the left to 60°N, 32°W on the right. The display shows the PV distribution (shaded with contour values of 0, 1, 1.5, 2, 4, 6, 8, and 12 PVU), the potential temperature (dashed contours at 5-K intervals), and the alongfront wind component (continuous isolines at 5 m $s^{-1}$ intervals). The tick marks on the abscissa are approximately 70 km apart, and further details of the dataset are given in section 3.

Now consider briefly the linkage between PV frontal pattern and the more standard frontal parameters of enhanced lateral shear, stratification, and baroclinicity. To illustrate the nature of the linkage we assume a steady unidirected flow field aligned along the $y$ axis of an $f$ plane. For this configuration and with $\theta$ as the vertical coordinate, the hydrostatic Ertel potential vorticity and its gradient on an isentropic surface are given, respectively, by

$$\mathrm{PV} = \left(\frac{\partial v}{\partial x_\theta} + f\right)[S]^{-1} \tag{2.1}$$

and

$$\frac{\partial \mathrm{PV}}{\partial x_\theta} = \left\{\left(\frac{\partial^2 v}{\partial x_\theta^2}\right) + (\mathrm{PV})\frac{\partial [S]}{\partial x_\theta}\right\}[S]^{-1}, \tag{2.2}$$

while the variation of the flow field with $\theta$ is given without further approximation by the geostrophic relation

$$\frac{\partial v}{\partial \theta} = \frac{1}{f}\frac{\partial \pi}{\partial x_\theta}. \tag{2.3}$$

Here the $\theta$ subscript refers to derivatives along an isentropic surface, the parameter $S$ is an inverse measure of the stratification such that $[S] = -(1/g)\partial p/\partial\theta$, $\Pi = c_p(p/p_0)^{R_d/c_p}$ denotes the Exner function, and $v$ will be regarded as the alongfront velocity.

It follows from Eq. (2.2) that large $\nabla_\theta$PV will prevail in a region that exhibits strong variations of both lateral shear and stratification along the isentropic surfaces. Inspection of Figs. 1 and 2 indicates, in accord with Eq. (2.2), that for this particular event the domain of the PV front is delineated by the layer of isentropes penetrating the stratosphere on the lateral edge of the jet. (Note that a direct visual estimate of this location can be derived from inspection of the spatial density of the intersection of the $v$ and $\theta$ isolines in Fig. 1.) Furthermore Eq. (2.3), the equivalent of the thermal wind in the $\theta$ coordinate framework, implies that the jet will demark regions above and below it of significant variations of the Exner function along isentropic surfaces, and hence by implication the existence of regions of enhanced baroclinicity.

Hence in relation to more conventional frontal parameters the signature of a PV front connotes strong

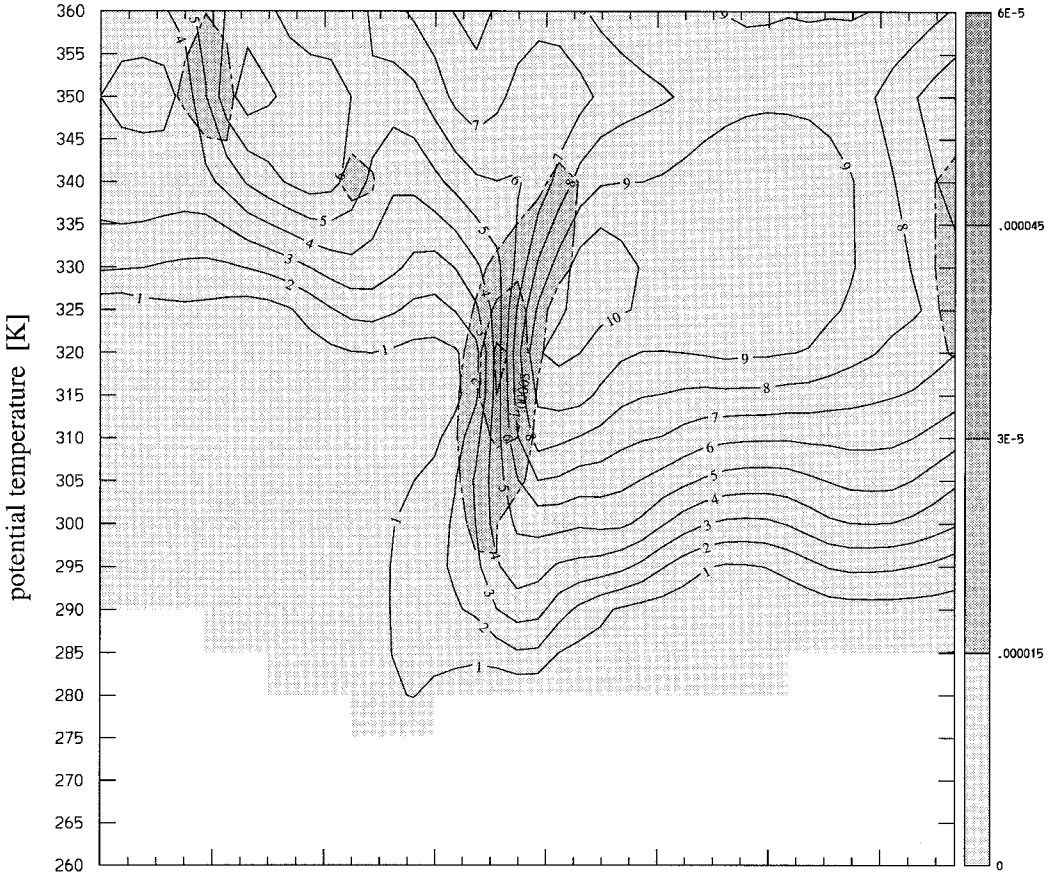


FIG. 2. Same cross section as for Fig. 1 but now with $\theta$ as vertical coordinate. The fields displayed are the potential vorticity and its gradient on isentropic surfaces. (The PV is shown with continuous contours at 1-PVU intervals, and the gradient is shaded with contour intervals of 0.15 PVU per 10 km.)

variations of lateral shear and stratification (along isentropic surfaces) on the edge of the jet stream, and enhanced baroclinicity above and below. We comment further on the issue of appropriate frontal parameters in section 4.

### *b. PV frontogenesis*

A tentative rationale for the concept of PV frontogenesis on isentropic surfaces can be derived by analogy with potential temperature frontogenesis at the earth's surface.

The analogy proceeds in two steps. First note that for inviscid adiabatic conditions the potential vorticity of an air parcel is conserved following the flow on an isentropic surface, that is,

$$\left(\frac{D}{Dt}\right)_\theta \mathrm{PV} = 0, \tag{2.4}$$

where the $(D/Dt)_\theta$ operator refers to the material derivative formulated on isentropic surfaces. Furthermore the strengthening of a PV front along, say the $y$ axis, can be assessed with the following reduced equation for $\nabla_\theta \mathrm{PV}$:

$$\left(\frac{D}{Dt}\right)_\theta \left(\frac{\partial \mathrm{PV}}{\partial x_\theta}\right) = -\left\{\left(\frac{\partial \mathrm{PV}}{\partial x_\theta}\right)\left(\frac{\partial u}{\partial x_\theta}\right) + \left(\frac{\partial \mathrm{PV}}{\partial y_\theta}\right)\left(\frac{\partial v}{\partial x_\theta}\right)\right\}. \tag{2.5}$$

In a simple flow setting the first of the two frontogenetical forcing terms on the right-hand side can be related to a horizontal deformation field acting on a two-dimensional potential vorticity distribution $\mathrm{PV} = \mathrm{PV}(x, \theta)$. {The analogy here is with deformation-induced surface frontogenesis [cf. Bergeron (1928)].}

Pursuing the analogy further, consider a deformation field acting on an initial atmospheric structure resembling the mean and longitudinally averaged Northern Hemisphere wintertime fields. The latter is depicted in a latitude–pressure section in Fig. 3, and in a latitude–$\theta$ section in Fig. 4. Coinspection of these figures again confirms that the domain of large $\nabla_\theta \mathrm{PV}$ is located near and poleward of the jet stream, and also that within the troposphere and lower stratosphere the region of larger $\nabla_\theta \mathrm{PV}$ is confined to the so-called middle world (Shaw

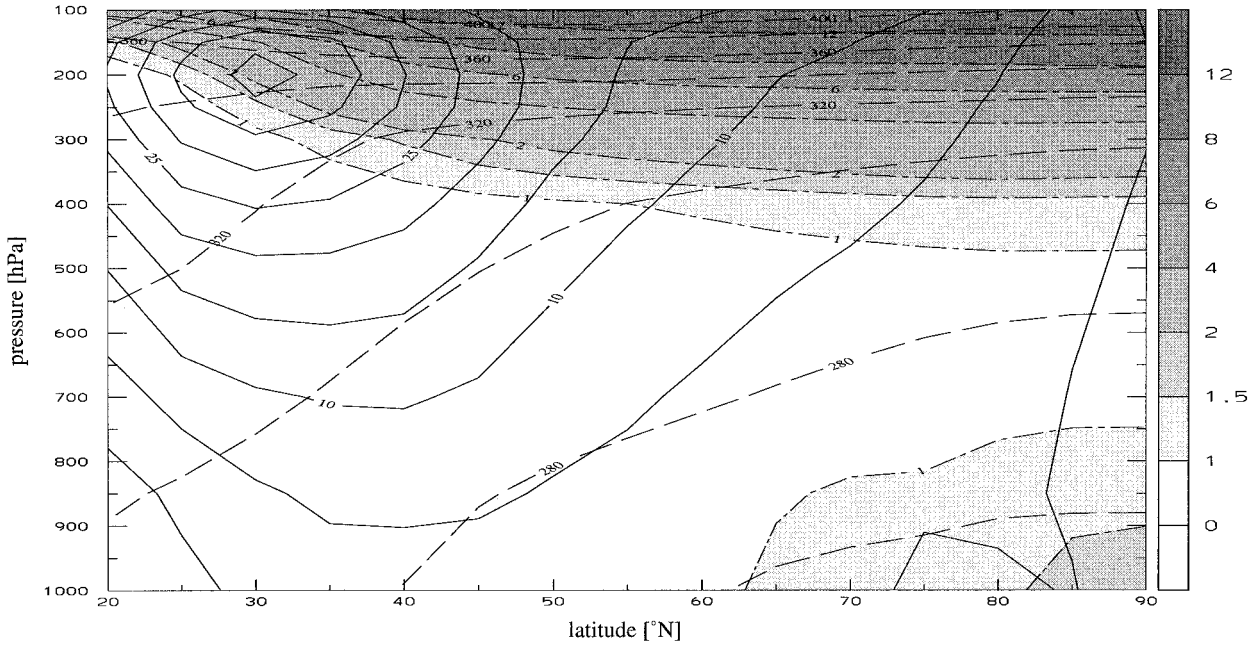


FIG. 3. A latitude–height section of the winter-mean (DJF) longitudinally averaged distribution of the potential temperature, zonal mean flow, and potential vorticity. The plotting convention as for Fig. 1 except that $\theta$ is now displayed at 20-K intervals. Data are the ECMWF analysis fields for the 1978–88 period [see Hoskins et al. (1989)].

1930; Hoskins 1991) defined by the layer of tropopause-transecting isentropes. It follows that a pure deformation-induced scale contraction can only yield significant PV frontogenesis within the middle world.

The second step in the analogy is related to classical baroclinic instability studies. These demonstrate that unstable wave perturbations growing on a basic state comprising the mean atmospheric structure (Figs. 3 and 4) will evolve to yield a family of cyclones and anticyclones with attendant realistic surface and upper-level fronts. From a PV perspective the evolving perturbations are viewed as the interaction of two spatially dis-

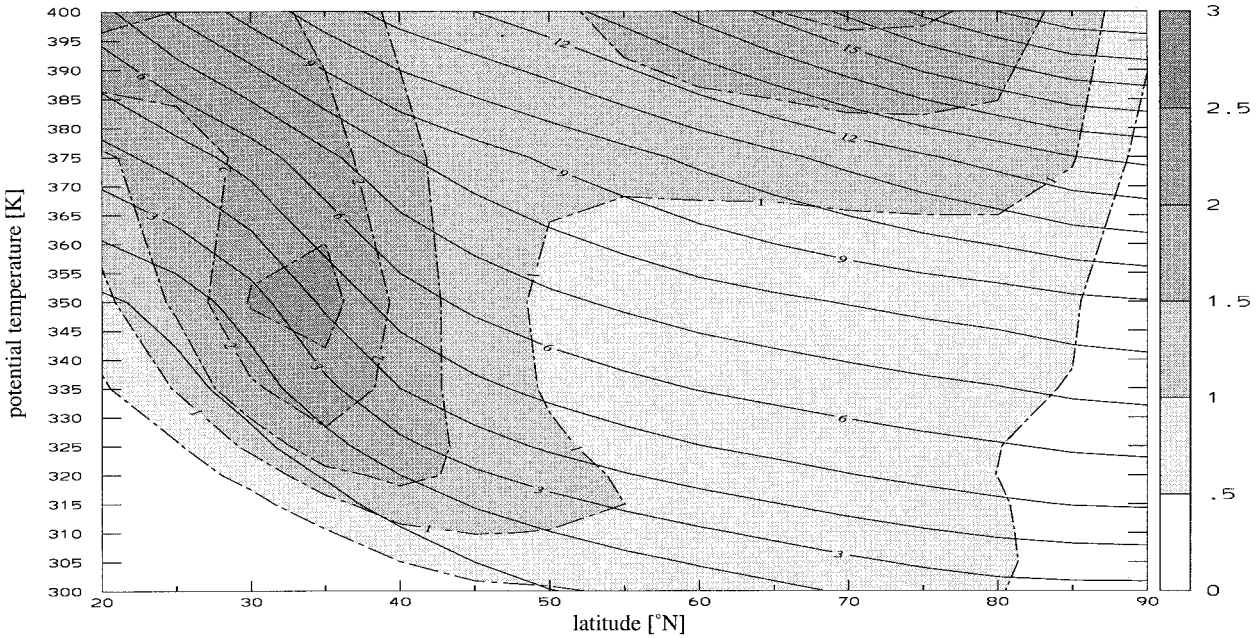


FIG. 4. The analog of Fig. 2 but for the Northern Hemisphere winter-mean (DJF) PV distribution in a latitude–$\theta$ section. (Note that the contour interval for the gradient is now 30 times smaller, that is, 0.5 PVU per 1000 km, and that the vertical scale only commences at 300 K.)

tinct elements—thermal perturbations on the surface baroclinic zone, and potential vorticity undulations within the forementioned middle world. In this setting *surface* frontogenesis is attributable to the deformation-induced scale contraction of a segment of the baroclinic zone to yield a strip of strongly enhanced baroclinicity at the surface, and the *upper-level* counterpart is the scale contraction of a segment of the potential vorticity undulation to form an interior band of sharpened PV gradient on the tropopause-transcending isentropic surfaces (cf. Figs. 1 and 2). Note that the frontal values of $\nabla_\theta$PV (Fig. 2) are almost two orders of magnitude larger than the climatological values (Fig. 4). (Note the change in the contour interval for $\nabla_\theta$PV.) Further ingredients of the analogy would be to relate different types of surface and upper-level fronts to related differences in the ambient atmospheric flow (Davies et al. 1991). We comment further on this point in the final section.

## 3. A case study of PV frontogenesis

### *a. A diagnostic framework*

The strategy here is to adopt the PV gradient on interior isentropic surfaces (i.e., $\nabla_\theta$PV) as an appropriate parameter to define upper-level fronts, and concurrently to regard its Lagrangian tendency as a diagnostic index of frontogenetic forcing.

The equation(s) for, and interpretations of, the PV tendency can be derived by analogy with the formulas for the baroclinicity indices of surface frontogenesis [see, e.g., Petterssen (1936), Lalaurette et al. (1994), Davies (1994)]. The pertinent equation(s) take the form

$$\left(\frac{D}{Dt}\right)_\theta \frac{1}{2}(\nabla_\theta \mathrm{PV})^2 = -(\nabla_\theta \mathrm{PV})^2\left(\frac{\partial v}{\partial n}\right), \qquad (3.1a)$$

or equivalently

$$= \frac{1}{2}(\nabla_\theta \mathrm{PV})^2[D\cos 2\delta - (\nabla\cdot\mathbf{v})_\theta]. \qquad (3.1b)$$

Here ($s$, $n$) prescribe a local Cartesian framework such that $s$ is aligned along a PV isoline with $n$ pointing toward high PV values, and $v$ is the velocity component in the $n$ direction. Also $D$ is the total deformation of the horizontal flow field and $\delta$ is the local angle between the dilatation axis and the PV isoline. The vector invariant form, [i.e., Eq. (3.1b)], serves to emphasize the role of deformation and horizontal divergence.

In the geostrophic limit the contribution due to the horizontal divergence vanishes, and the equation can be recast in a more restrictive form [cf. Hoskins et al. (1978)],

$$\left(\frac{D}{Dt}\right)_\theta (\nabla_\theta \mathrm{PV}) = \mathbf{Q}_{\mathrm{PV}}, \qquad (3.2a)$$

where

$$\mathbf{Q}_{\mathrm{PV}} = |\nabla_\theta \mathrm{PV}|\left[\mathbf{k}\times\left(\frac{\partial \mathbf{v}_g}{\partial s}\right)\right]. \qquad (3.2b)$$

The utility of the foregoing PV frontogenesis equations [(3.1)–(3.2)] will hinge upon their ability to identify the occurrence, and to shed light upon the dynamics, of the principal PV frontal zone(s). A quantitative evaluation of the Lagrangian tendency can be obtained by direct calculation of the forcing term in Eq. (3.1). A qualitative appraisal of the frontogenesis can be ascertained from Eq. (3.2a,b) by adapting the method used to interpret the conventional baroclinicity-based **Q** vector (Hoskins et al. 1978; Sanders and Hoskins 1990). This entails the following sequence of steps: 1) visual inspection of the wind and PV fields on an appropriate isentropic chart to locate the regions of large PV gradients, 2) deduction of the direction of the gradient of horizontal velocity field along the PV isolines in the pinpointed regions, and 3) a surmise of the relative strength and the direction of $\mathbf{Q}_{\mathrm{PV}}$. [Note that (div$\mathbf{Q}_{\mathrm{PV}}$), unlike its conventional counterpart, does not constitute a contribution to the forcing of vertical motion.]

Thus this approach, based upon Eqs. (3.1)–(3.2), seeks to build upon and explore further the analogy drawn in the previous section between surface baroclinic frontogensis and internal PV frontogenesis on middle-world isentropic surfaces.

### *b. The frontal event*

Our limited objectives here are to examine the possibility of detecting PV frontogenesis with conventionally available datasets, and thereby to concurrently test the utility of the foregoing type of diagnosis. The study is undertaken with data derived from the 6-h operational analysis cycle of the ECMWF, and the suite provides model data at a horizontal resolution of approximately 60 km in midlatitudes with a vertical resolution at tropopause levels of about 25 hPa. (The dataset is internally consistent and is representative of a state-of-the-art analysis set for numerical weather prediction. It incorporates conventional surface and upper-air soundings as well as satellite-based information, but the stringent time constraints placed upon the analysis cycle mean that some data are not included.)

The event to be considered occurred in the mid-Atlantic and evolved late on 21 November 1992. It developed on the western flank of an upper-level trough, and the trough itself was linked with, and located upstream of, a major quasi-stationary surface cyclone off Iceland. The frontal cross sections displayed in Figs. 1 and 2 pertain to a late phase of this event, and the section's location is marked in Fig. 7d.

#### 1) ASPECTS OF THE STANDARD ANALYSIS

Figure 5 shows a sequence of 6-h charts for the 400-hPa surface from 1800 UTC 21 November to 1200 UTC

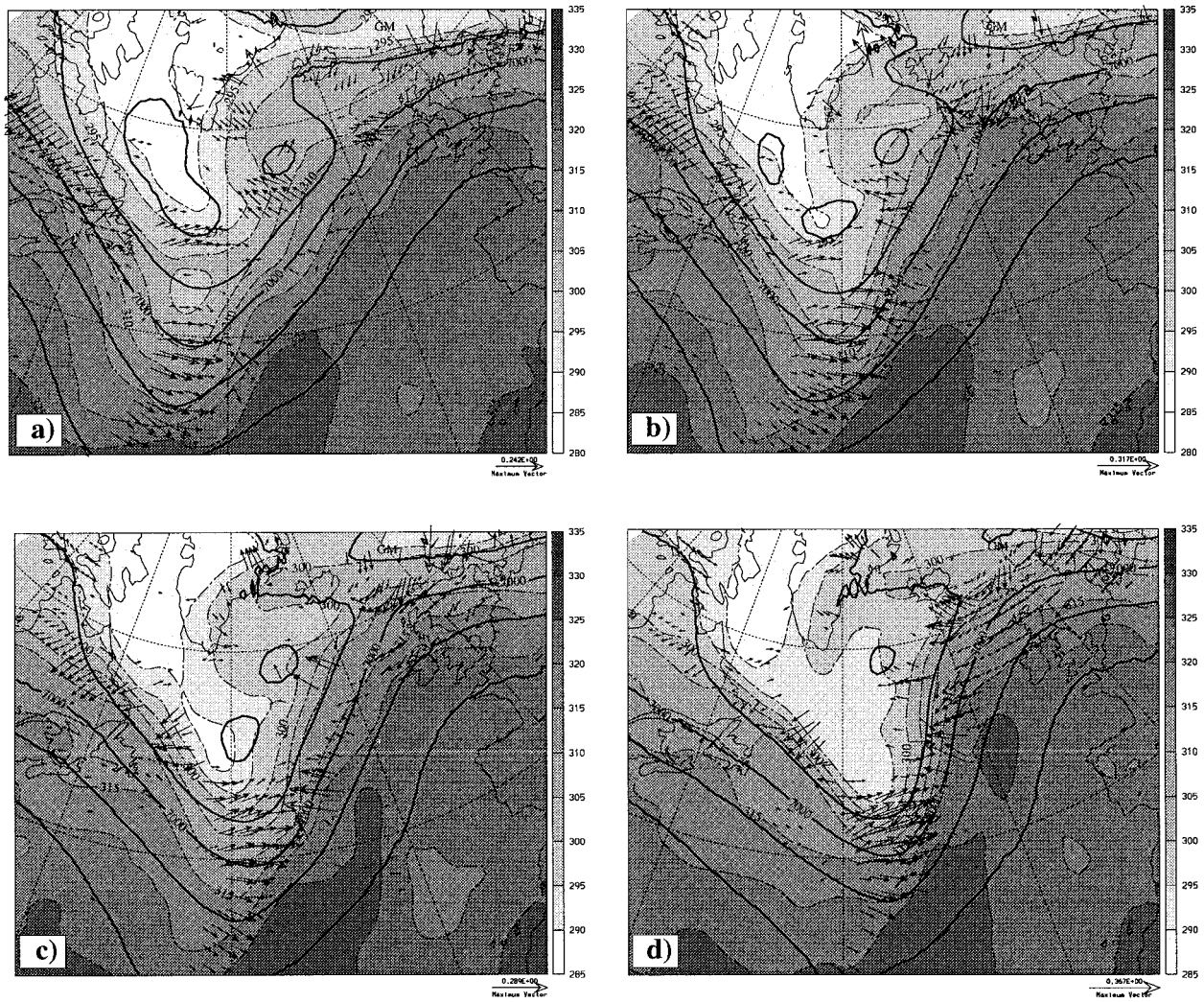


FIG. 5. A 6-h sequence of 400-hPa charts from 1800 UTC 21 November to 1200 UTC 22 November 1992. Depicted are the geopotential height field (bold continuous isolines, contour interval of 200 m) and the potential temperature pattern (shaded and with dashed isolines, contour interval every 5 K), and the major **Q** vectors (values plotted only if they exceed 0.02 K per 6 h per 100 km).

22 November. The fields displayed are the geopotential height, the potential temperature, and the conventional two-dimensional **Q** forcing vectors.

At this pressure level the height pattern comprises a sharp bow-shaped trough that moves slowly eastward during the 18 h of the sequence. The thermal front under consideration evolves within an initially weak baroclinic zone on the western flank of the trough. It intensifies rapidly during the second half of the period, and at the final time extends around the base of the trough. The **Q** field is highly structured with a translating pattern of frontogenetic forcing on the trough's western flank and sustained forcing at its base. The associated div**Q** pattern (recall that only the large-amplitude **Q** vectors are plotted in Fig. 5) equates to the contribution of the quasi-geostrophic forcing at 400-hPa level to the ageostrophic flow. The inference is that the two forementioned **Q**-field patterns connote a tendency for ascent (descent) in the domain to the tip (rear) of the band of displayed vectors, and this in turn would imply a highly structured forcing of the vertical velocity field.

It is not our objective here to present a detailed analysis of the evolution of the thermal front at 400 hPa, but further aspects of thermal frontogenesis are considered in section 4.

### 2) THE PV APPROACH

An indication of the spatial scale and temporal evolution of the PV frontogenesis that accompanied this frontal event can be gleaned from inspection of Figs. 6 and 7. The charts are for the 315-K isentropic charts and display, for the same 6-h sequence as Fig. 5, the PV pattern plus the horizontal wind field (Fig. 6), and

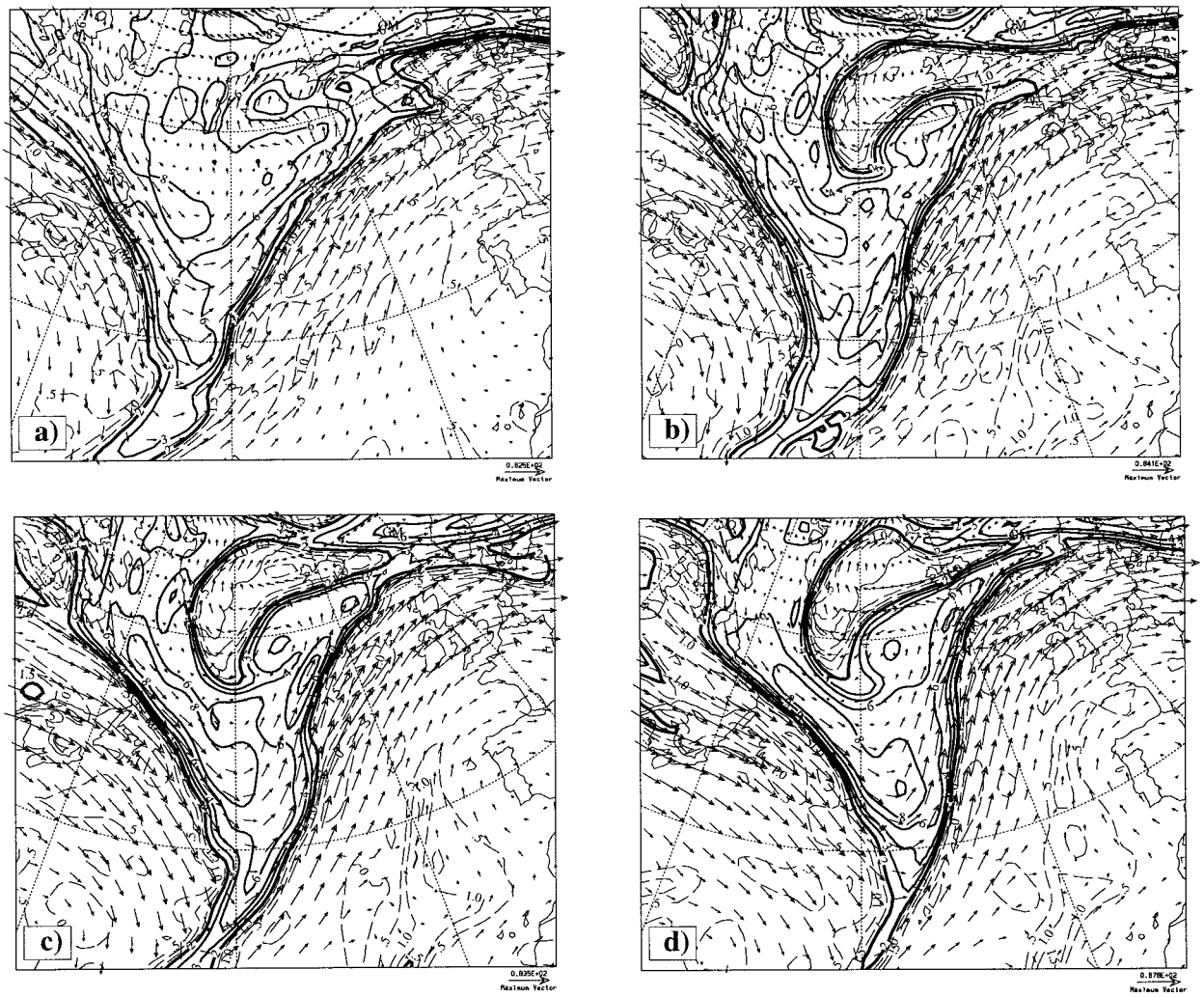


FIG. 6. The same time sequence as Fig. 5, but now the fields depicted are the PV distribution and the flow field on the 315-K isentropic surface. The potential vorticity is displayed with dashed contours at 0.5-PVU intervals for PV up to 2 PVU, and thereafter for values of 2, 3, 4, 6, 8, 12, and 16 PVU. The maximum wind vectors in the various panels vary from 83 to 90 m $s^{-1}$.

the Lagrangian tendency of the PV frontogenesis index (Fig. 7).

Again we focus on the western flank of the trough/major equatorward-extending PV incursion. Figure 6 reveals that significant lateral scale contraction occurs on this flank along a zone delineated by the 2–8-PVU isolines, and that this results in a marked strengthening of the associated gradient. This is verified in Fig. 7, which shows that the region of significant PV frontogenetic forcing [see Eqs. (3.1a) and (3.1b)] takes the form of a narrow translating band confined to the aforementioned PV interval. The forcing is only evident in the latter half of the considered time period.

Qualitative appraisal of the PV frontogenesis, based upon an assessment of the $\mathbf{Q}_{\mathrm{PV}}$ pattern [see Eqs. (3.2a) and (3.2b) and the accompanying discussion], suggests that a key role is played by the elongated subsynoptic-scale PV anomaly of strength approximately 8 PVU located alongside the emerging front and embedded within the larger synoptic-scale PV undulation. In effect the sustained PV frontogenesis is linked to the scale contraction within the confluent isolines of PV immediately upstream of the anomaly with a weaker reverse effect downsteam. The front also appears to move in tandem with the anomaly and this suggests significant relative movement of the air through the frontal zone. Later in the evolution of the system both the frontal zone and the PV anomaly traverse around the base of the trough onto its forward flank.

The direct inference is that the PV frontogenesis equation captures a distinct event of frontogenesis that results in an elongated band of enhanced $\nabla_\theta$PV on the 315-K isentrope. A similar signal is evident on charts (not shown) for other middle-world isentropes.

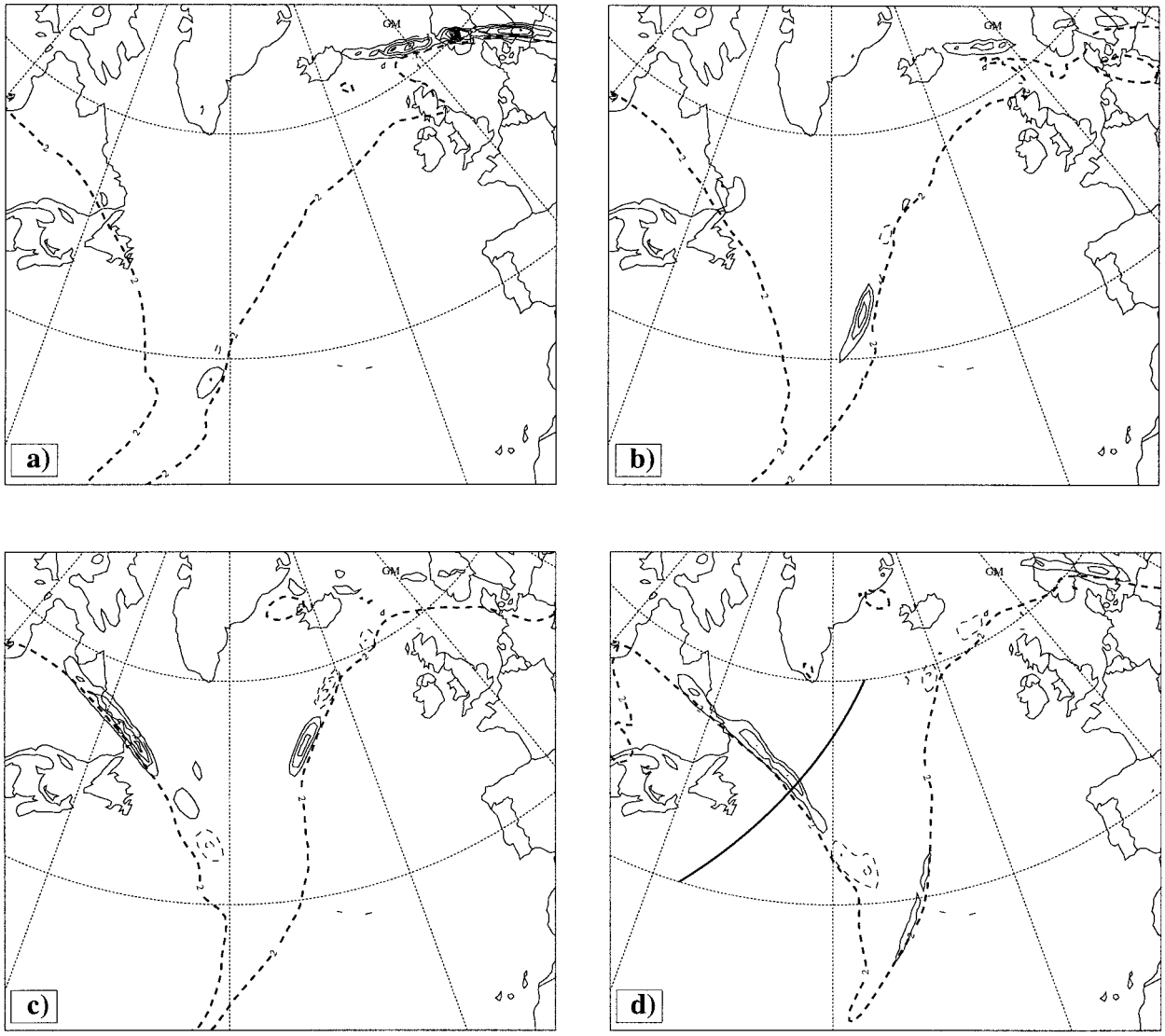


FIG. 7. As for Fig. 6, but the displayed field is that of the PV frontogenetic forcing [contour interval of 0.1 PVU$^2$ per 10 km$^2$ per 6 h; see Eqs. (3.1a) and (3.1b)]. For reference the location of the 2-PVU isoline is also displayed on each chart as a bold dashed line. [In (d) the bold continous line denotes the location of the cross section for Figs. 1 and 2.]

## 4. A contrast of diagnostic approaches

In the present study upper-level fronts and frontogenesis have been viewed from a PV perspective. The resulting twin concepts of a PV front and PV frontogenesis were adopted as an alternative approach for diagnosing fronts and interpretating upper-level frontogenesis. Here we append some brief remarks on the merits and limitations of extant techniques alongside a similar critique of the alternative approach. To this end consider in turn the demarkation of the frontal zone and the diagnosis of frontogenesis.

### *a. Demarkation of fronts*

Reappraisal of Fig. 1 indicates that the conventional frontal parameters of baroclinicity, lateral shear, and vertical stratification attain their respective extrema at disparate locations. This disparity is a characteristic of upper-level fronts, and moreover there is an incomplete spatial overlap of the domains defined by locally enhanced values of the individual parameters. (For example the baroclinicity vanishes at the level of the jet, although the lateral shear attains its peaks value in the vicinity.) One inference is that the conventional frontal parameters do not individually define the entire frontal zone.

In an attempt to counter this seeming shortcoming, a range of more refined indices have been proposed to identify the zone. These include the baroclinicity plus the vertical stratification (Nyberg and Palmén 1942; Berggren 1952), the potential vorticity structure (Reed

and Sanders 1953; Reed 1955; Reed and Danielsen 1960), the baroclinicity plus the acrossfront lateral shear (Shapiro 1976); the combination of the baroclinicity, the vertical stratification, and the vertical and lateral shear (Newton and Trevisan 1984a); the so-called absolute momentum of the alongfront flow component [see, e.g., Eliassen (1990); Shapiro and Keyser (1990)]. The variety of indices and the contention (Shapiro and Keyser 1990) that it is only the absolute momentum that captures the entire frontal domain emphasizes the inherent difficulty of defining such a single parameter. Indeed it raises the issue of the appropriateness or otherwise of such a quest.

In relation to the present study we note that demarcation of the frontal zone has been linked to stratospheric intrusions and coherent PV anomalies (Reed and Sanders 1953; Reed 1955), the boundaries of the frontal zone have been equated to quasi discontinuities of potential vorticity on a $\theta$ surface (Reed and Danielsen 1960), and that the midtropospheric portion of the frontal zone is not delineated by such discontinuities (Shapiro and Keyser 1990).

The $\nabla_\theta$PV parameter of the present study is another PV-related index. Its domain of enhanced values (see Figs. 1 and 2) does demark a coherent transtropopause structure, but it too does not include the lowest portion of the traditional frontal region. The latter mismatch stems from two fundamental features of PV frontogenesis. First the ($\nabla_\theta$PV) parameter does not relate directly to the baroclinicity [Eqs. (2.1)–(2.3)], but only connotes, as indicated earlier, that enhanced baroclinicity will be present at levels above and below the main PV front. Second, the parameter refers only to the internal PV front and its associated flow signal. From a PV perspective the realized structure of the front is the net of the signal to be attributed to ($\nabla_\theta$PV) and the surface plus free-atmosphere signal associated with the surface $\nabla\theta$ front.

### *b. Diagnosis of frontogenesis*

A diagnostic analysis of frontogenesis should account for the space–time structure of the front, and also offer insight on the underlying dynamics.

#### 1) ASPECTS OF A CONVENTIONAL APPROACH

The customary approach has been to focus on the enhancement of the baroclinicity. To overview the ingredients of such an approach, consider the frontogenetic equation for the gradient of the potential temperature on a pressure surface, that is, $(\nabla_h\theta)_p$. For adiabatic motion this equation can be written in the form [cf. Petterssen (1936)]

$$\left(\frac{D}{Dt}\right)_p \frac{1}{2}(\nabla_h\theta)_p^2 = \frac{1}{2}(\nabla_h\theta)_p^2\,[D_p\cos 2\delta - (\nabla\cdot\mathbf{v}_h)_p] - \left(\frac{\partial\theta}{\partial p}\right)[(\nabla_h\theta)_p\cdot(\nabla_h\omega)_p]. \quad (4.1)$$

Here, the notation is as before but with the subscript $p$ signifying operations on a pressure surface.

A kinematic analysis based upon Eq. (4.1) requires an evaluation of the individual frontogenetic forcing terms, namely, the two-dimensional deformation-induced scale contraction of baroclinicity on pressure levels, the contribution of horizontal convergence, and the tilting of isentropes by the $\omega$ vertical velocity field. In addition the Lagrangian tendency of $|\nabla_h\theta|_p$ includes the vertical advection of baroclinicity onto or away from a specific pressure level. All these effects are linked directly or indirectly to $\omega$, and thus a knowledge of the four-dimensional distribution of this derived variable is central to the diagnosis. This in turn requires high-resolution observational (or modeled) data for the accurate evaluation of $\omega$.

Qualitative understanding of $|\nabla_h\theta|_p$ frontogenesis has often been sought within the quasigeostrophic framework. Integral to this framework is the dual role indicated earlier for the **Q** field; that is, it is a measure of the frontogenesis on a pressure surface and an indicator of the forcing of the vertical velocity. For instance the translating **Q**-field signature on the western flank of the trough in Fig. 5 denotes frontogenetic scale contraction, whereas the associated pattern of div**Q** is indicative of a tendency for a counteracting frontolytic-inducing vertical circulation comprising ascent (descent) on the warm (cold) side of the front. In contrast the cooling within the core of the trough itself (cf. Figs. 5c,d) cannot be accounted for by single level advection or scale contraction, and is therefore suggestive of an indirect frontogenetic larger-scale ascent.

A subtle interplay of the two effects of scale contraction and tilting is central to one interpretation of the baroclinicity enhancement [see, e.g., Shapiro and Keyser (1990), Rotunno et al. (1994), and the references therein]. In this interpretation, upper-level frontogenesis is viewed as the result of a sequence of phases such that the two effects contibute constructively immediately upstream of the trough's axis to force an indirect transverse frontal circulation and rapid frontogenesis, whereas both farther upstream and downstream the two contributions can significantly counter one another.

The recognition that the quasigeostrophic framework is not appropriate in regions of strong tropopause undulations has prompted the development of more sophisticated (and more complex) diagnostic procedures based upon a refined decomposition of the $\omega$ field and/or explicit incorporation of curvature effects [see, e.g., Newton and Trevisan (1984a,b); Reeder and Keyser (1988); Keyser et al. (1988); Cammas and Ramond

(1989); Sanders et al. (1991); Keyser et al. (1989, 1992); Lalaurette et al. (1994)].

### 2) THE PV APPROACH

The ingredients of this approach are evident in PV frontogenesis Eqs. (3.1)–(3.2). The former equation has two forcing terms, and the latter quasigeostrophic form only one. Also there is no advection of enhanced $\nabla_\theta$PV away from or onto an isentropic surface.

The evolution of PV frontogenesis can be computed using Eq. (3.1), appraised qualitatively (unhampered by the need to estimate counteracting effects) using Eq. (3.2), and discerned readily and unambiguously on charts (or time loops) that display the PV distribution on isentropic surfaces.

However, the approach has both observation-oriented and conceptual limitations. In comparison with conventional frontal parameters, the parameter $\nabla_\theta$PV is a much more complex and highly derived quantity. Its evaluation requires accurate high-resolution data. (Its computation, but not its accuracy, is facilitated by the availability of gridded NWP datasets).

Another ingredient that complicates, and detracts from, a direct interpretation of PV frontogenesis is the possible nonconservation of PV during the development. This can be associated with physical factors (radiative effects, meso- and smaller-scale irreversible mixing, and cloud diabatic processes), observational factors (inadequate or inaccurate data), and numerical factors (defects in interpolation or space–time integration schemes of the analysis). These limitations are exacerbated by the strong scale contraction that prevails during frontogenesis. The evaluation or eradication of these factors certainly merits attention, but a comparison of the degree of nonconservation (Fig. 6) with the calculated values of frontogenetic forcing (Fig. 7) suggests that the effects of nonconservation at most modulate rather than dominate the diagnosis.

A major conceptual and practical drawback is that the PV approach does not incorporate direct information on the vertical motion or displacement. (Recall that in contrast to the conventional **Q** field, the $\mathbf{Q}_{\rm PV}$ field does not carry dual information.) Notwithstanding the influence of the frontogenesis upon both stratosphere–troposphere exchange and surface weather is initimately linked to the vertical displacement and development of stratospheric intrusions. A partial and qualitative remedy for this deficiency can be obtained by considering the evolution of the gradient of PV with respect to $\theta$, that is, $(\partial \mathrm{PV}/\partial\theta)$. During PV frontogenesis the positive ambient value of $\partial \mathrm{PV}/\partial\theta$ reduces toward 0 within the core of the PV front, and with the onset of an intrusion it reverses sign below and above this core (cf. Figs. 1 and 2). Thus the value, and the Lagrangian tendency, of $\partial \mathrm{PV}/\partial\theta$ can help to indicate the location and rate of development of an intrusion, and thereby provide indirect information on the vertical motion. This parameter's Lagrangian tendency is given by

$$\left(\frac{D}{Dt}\right)_\theta\left(\frac{\partial \mathrm{PV}}{\partial\theta}\right) = -\left[\left(\frac{\partial u}{\partial\theta}\right)\left(\frac{\partial \mathrm{PV}}{\partial x_\theta}\right) + \left(\frac{\partial v}{\partial\theta}\right)\left(\frac{\partial \mathrm{PV}}{\partial y_\theta}\right)\right], \quad (4.2a)$$

$$= -\left(\mathbf{v}_T\cdot\frac{\partial}{\partial s_\theta}\right)\mathrm{PV}, \quad (4.2b)$$

where $\mathbf{v}_T = (\partial u/\partial\theta, \partial v/\partial\theta)$. Hence, the tendency is determined by the rate of change of the potential vorticity along the direction of the pseudo–thermal wind field $\mathbf{v}_T$.

The approximate value of the tendency can be readily assessed by coinspection of the fields of the Exner function ($\Pi$) and the potential vorticity (PV) on the same isentropic chart. This follows from noting that (a) on replacing $\mathbf{v}_T$ by its geostrophic equivalent, Eq. (4.2a) and (4.2b) reduce to the form

$$\left(\frac{D}{Dt}\right)_\theta\left(\frac{\partial \mathrm{PV}}{\partial\theta}\right) = -\left\{\left(-\frac{\partial \Pi}{\partial y_\theta}\right)\left(\frac{\partial \mathrm{PV}}{\partial x_\theta}\right) + \left(\frac{\partial \Pi}{\partial x_\theta}\right)\left(\frac{\partial \mathrm{PV}}{\partial y_\theta}\right)\right\}$$

$$= -J\left[\left(\frac{\Pi}{f}\right), \mathrm{PV}\right], \quad (4.2c)$$

and (b) the amplitude of the Jacobian term in Eq. (4.2c) is given by the spatial density of the intersection of the isolines of $\Pi$ and PV. (Note that in the quasigeostrophic limit $\partial \mathrm{PV}/\partial\theta$ is proportional to $\nabla^2\Pi$, and hence its Lagrangian tendency is linked to the field of $\nabla^2\omega$.)

A cursory assessment of the potential utility of Eq. (4.2c) can be gleaned from Fig. 8. The figure's panels are 315-K isentropic charts for 0600 UTC 22 November (cf. Fig. 6c), and display, respectively, (a) the distributions of $\Pi$ and PV both plotted at equal contour intervals, and (b) the $\omega$ field extracted from the ECMWF analysis. Comparison indicates a not unreasonable qualitative agreement with corresponding dipoles of ascent and descent located far upstream of the trough axis and at its base.

### 3) ADDITIONAL REMARKS

Our objective has been to profer an alternative to, rather than to supplant, the conventional diagnostic approach to studying upper-level fronts and frontogenesis. Key differences between the two approaches relate to the selection of frontal indices, the completeness and dynamical simplicity of the diagnostic analysis, and the ensuing perceived nature of the frontogenesis. Here we comment on these points, placing the emphasis on consideration of the present approach.

In the PV approach the diagnostic analysis centers on a single parameter $\nabla_\theta$PV. It is used to denote the frontal location, and its Lagrangian tendency adopted as a diagnostic measure of frontogenesis. Thus this approach circumvents, without solving, the thorny issue of defin-

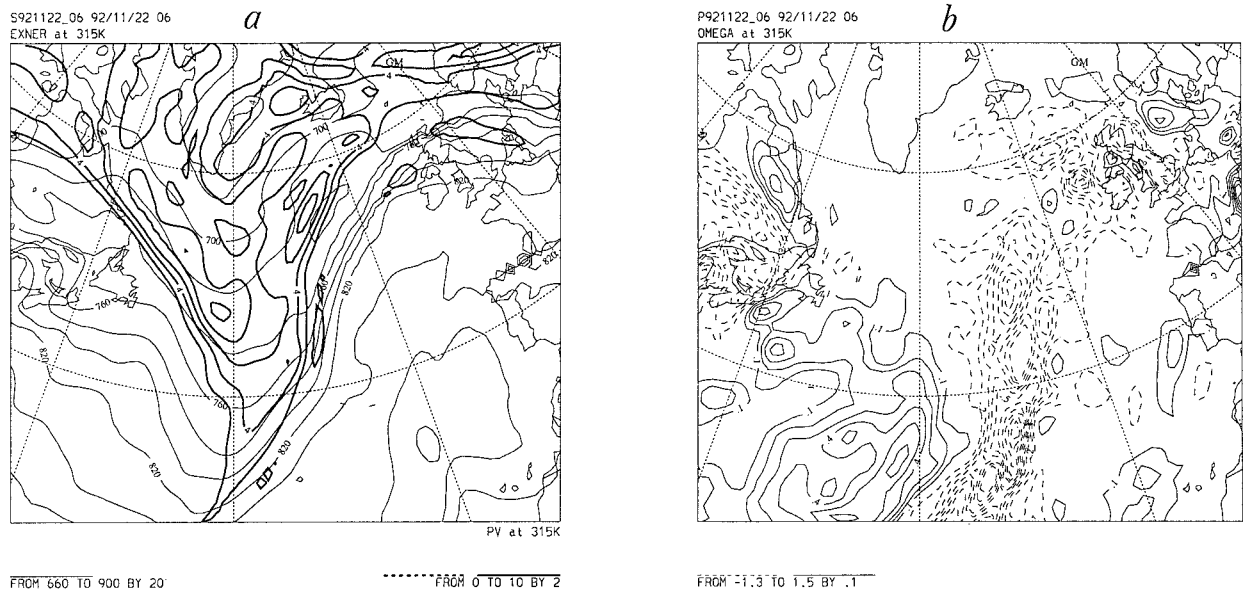


FIG. 8. Isentropic charts for the 315-K surface at 0600 UTC 22 November. (a) The distributions of the Exner function (Π) and the potential vorticity (PV) both plotted at equal contour intervals. (b) The $\omega$ field as extracted from the ECMWF analysis.

ing a single or multivariable frontal parameter that demarks the entire vertically coherent frontal structure.

The utility of the $\nabla_\theta$PV parameter can also be compared with other extant indices. A related index is the gradient of potential temperature on a suitable PV surface (say, PV = 2), or more appropriately in view of Fig. 2 on a band of PV surfaces (say $1.5 < \text{PV} < 8$). This index's utility is further limited by the nonmonotonicity of PV with height during tropopause fold events. Also, in comparison with the absolute momentum index referred to earlier, we note that the ($\nabla_\theta$PV) parameter retains its dynamical utility within the strongly three-dimensional setting of upper-level fronts, whereas strong curvature effects would require consideration of angular momentum.

The PV approach (unlike the standard approach) is incomplete in that it does not address directly the vertical displacement of air parcels within the evolving front. For example, the development and vertical penetration of stratospheric intrusions is not deduced directly from the PV dynamics, but this limitation can be alleviated somewhat by studying the evolution of $\partial$PV/$\partial\theta$. Notwithstanding the decoupling of the PV approach from consideration of the vertical velocity the approach does result in a comparatively simple analysis of the frontogenesis.

The foregoing difference in emphasis also spills over into the interpretation of the frontogenesis itself. The standard approach attributes frontogenesis to the subtle interplay of scale contraction on a pressure surface and the tilting of isentropes onto that surface by the vertical velocity field. Such an interplay cannot prevail at the earth's surface since the tilting effect vanishes, and one inference is that upper-level frontogenesis is dynamically distinct from its surface counterpart. In contrast the PV approach seeks to establish an analogy betwen the two phenomena, and the results of the case study lend credence to the idea.

## 5. Further remarks

This study has outlined an alternative view of upper-level frontogenesis that is based upon a potential vorticity (PV) perspective. In this approach frontogenesis is viewed as the enhancement of the PV gradient on the tropopause-transcending isentropic surfaces of the ''middle world.'' The theoretical considerations (section 2) suggest that the approach is physically meaningful, and the results of the case study and discussion (sections 3 and 4) indicate that it provides a transparent, albeit incomplete, depiction of the physical phenomenon.

The results provide a pleasing correspondence between surface $\theta$ frontogenesis and upper-level PV frontogenesis, and this both helps undergird and exemplifies the ''PV–$\theta$'' view of atmospheric dynamics. It underlines the significance of the background PV distribution; the importance of the tropopause transcending isentropes of the middle world; and the development, and indeed the existence, of a narrow elongated band undergoing PV frontogenesis.

The approach also has the potential to offer further insight on the dynamics of the upper-level fronts and related phenomena. The analyses indicate the cooccurrence of a subsynoptic PV anomaly embedded within the stratosphere and an attendant jet streak [cf. Mattocks and Bleck (1986); Bluestein (1993)], and the $\mathbf{Q}_{\text{PV}}$ component of the analysis suggests that these features might be significant for the PV frontogenesis. This also

prompts questions related to the frequency of occurrence, spatial scale, and origin of these stratospheric PV anomalies.

The occurrence of PV frontogenesis is indicative of a sharpening and maintenance of the midlatitude tropopause break. Such a process relates to, but differs somewhat from, two hypotheses regarding the tropopause. The first postulates that baroclinic eddies act to homogenize the PV within the troposphere (Lindzen 1993). Potential vorticity frontogenesis can contribute to such a process within the middle world, but the emphasis of the present interpretation is on the enhancement of $\nabla_\theta$PV at the tropopause break. The second and related hypothesis is that the self-same eddies act to maintain the entire extratropical tropopause. Again PV frontogenesis can contribute to this maintenance by sharpening the PV gradient on either side of the break, and the break itself sustains the conduit for stratosphere–troposphere exchange.

It is also pertinent to note, by analogy with surface frontogenesis, that the nature of the upper-level fronts could be depend sensitively upon the structure of the ambient flow and in particular upon the lateral shear (see, e.g., Davies et al. 1991; Hines and Mechoso 1991). This points to the possibility of different types of upper-level fronts.

*Acknowledgments.* The authors wish to thank Dr. Heini Wernli for his unstinting support, and are indebted to Prof. D. Keyser for providing a detailed and penetrating review of an earlier version of this manuscript.

## REFERENCES

Berggren, R., 1952: The distribution of temperature and wind connected with active tropical air in the higher troposphere and some remarks concerning clear air turbulence at high altitude. *Tellus,* **4,** 43–53.

Bluestein, H. B., 1993: *Synoptic–Dynamic Meteorology in Mid-latitudes.* Vol. II. Oxford University Press, 594 pp.

Cammas, J.-P., and D. Ramond, 1989: Analysis and diagnosis of the composition of ageostrophic circulations in jet–front systems. *Mon. Wea. Rev.,* **117,** 2447–2462.

Davies, H. C., 1994: Theories of frontogenesis. *The Life Cycles of Extratropical Cyclones.* S. Gronas and M. A. Shapiro, Eds., Vol. I, University of Bergen, 182–192.

——, Ch. Schär, and H. Wernli, 1991: The palette of fronts and cyclones within a baroclinic wave development. *J. Atmos. Sci.*, **48,** 1666–1689.

Eliassen, A., 1990: Transverse circulations in frontal zones. *Extratropical Cyclones: The Erik Palmén Memorial Volume,* C. W. Newton and E. O. Holopainen, Eds., Amer. Meteor. Soc., 155–165.

Hines, K. M., and C. R. Mechoso, 1991: Frontogenesis processes in the middle and upper troposphere. *Mon. Wea. Rev.,* **119,** 1225–1241.

Hoskins, B. J., 1991: Towards a PV–$\theta$ view of the general circulation. Tellus, **43AB,** 27–35.

——, I. Draghici, and H. C. Davies, 1978: A new look at the $\omega$-equation. *Quart. J. Roy. Meteor. Soc.,* **104,** 31–38.

——, M. E. McIntyre, and A. W. Robertson, 1985: On the use and significance of isentropic potential vorticity maps. *Quart. J. Roy. Meteor. Soc.,* **111,** 877–946.

——, H.-H. Hsu, I. N. James, M. Masutani, P. D. Sardeshmukh, and G. H. White, 1989: Diagnostics of the global atmospheric circulation based upon ECMWF analyses 1979–1988. WMO/TD-No. 326.

Keyser, D., and M. A. Shapiro, 1986: A review of the structure and dynamics of upper-level frontal zones. *Mon. Wea. Rev.,* **114,** 452–499.

——, M. J. Reeder, and R. J. Reed, 1988: A generalization of Petterssen's frontogenesis function and its relation to the forcing of vertical motion. *Mon. Wea. Rev.,* **116,** 762–780.

——, B. D. Schmidt, and D. G. Duffy, 1989: A technique for representing three-dimensional vertical circulations in baroclinic disturbances. *Mon. Wea. Rev.,* **117,** 2463–2494.

——, ——, and ——, 1992: Quasi-geostrophic diagnosis of three-dimensional ageostrophic circulations in an idealized baroclinic disturbance. *Mon. Wea. Rev.,* **120,** 698–730.

Lalaurette, F., C. Fischer, and J.-P. Cammas, 1994: Location and interaction of upper- and lower-tropospheric adiabatic frontogenesis. *Mon. Wea. Rev.,* **122,** 2004–2021.

Lindzen, R. S., 1993: Baroclinic instability and the tropopause. *J. Atmos. Sci.,* **50,** 1148–1151.

Mattocks, C., and R. Bleck, 1986: Jet streak dynamics and geostrophic adjustment processes during the initial stages of lee cyclogenesis. *Mon. Wea. Rev.,* **114,** 2033–2055.

Newton C. W., and A. Trevisan, 1984a: Clinogenesis and frontogenesis in jet-stream waves. Part I: Analytic relations to wave structure. *J. Atmos. Sci.,* **41,** 2717–2734.

——, and ——, 1984b: Clinogenesis and frontogenesis in jet-stream waves. Part II: Channel model numerical experiments. *J. Atmos. Sci.,* **41,** 2735–2755.

Nyberg, A., and E. Palmen, 1942: Synoptische-aerologische Bearbeitung der internationalen Registrerballonaufsteige in Europa in der Zeit 17–19 Oktober 1935. *Statens Meteorol.-Hydrol. Anstalt, Medd., Ser. Uppsater,* No. 40, 1–43.

Petterssen, S., 1936: A contribution to the theory of frontogenesis. *Geofys. Publ.,* **11,** 1–27.

Reed, R. J., 1955: A study of a characteristic type of upper-level frontogenesis. *J. Meteor.,* **12,** 226–237.

——, and F. Sanders, 1953: An investigation of the development of a mid-tropospheric frontal zone and its associated vorticity field. *J. Meteor.,* **10,** 338–349.

——, and E. F. Danielsen, 1960: Fronts in the vicinity of the tropopause. *Arch. Meteor. Geophys. Bioklimatol.,* **11A,** 1–17.

Reeder, M. J., and D. Keyser, 1988: Balanced and unbalanced frontogenesis. *J. Atmos. Sci.,* **45,** 3366–3386.

Rotunno, R., W. C. Skamarock, and C. Snyder, 1994. An analysis of frontogenesis in numerical simulations of baroclinic waves. *J. Atmos. Sci.,* **51,** 3373–3398.

Sanders, F., and B. J. Hoskins, 1990: An easy method for estimation of Q-vectors from weather maps. *Wea. Forecasting,* **5,** 346–353.

——, L. F. Bosart, and Ch.-Ch. Lai, 1991: Initiation and evolution of an intense upper-level front. *Mon. Wea. Rev.,* **119,** 1337–1367.

Shapiro, M. A., 1976: The role of turbulent heat flux in the generation of potential vorticity in the vicinity of upper-level jet stream systems. *Mon. Wea. Rev.,* **104,** 892–906.

——, and D. Keyser, 1990: On the structure and dynamics of fronts, jet streams and the tropopause. *Extratropical Cyclones: The Erik Palmén Memorial Volume,* C. W. Newton and E. O. Holopainen, Eds., Amer. Meteor. Soc., 167–191.

Shaw, N., 1930: *Manual of Meteorology.* Vol. III. *The Physical Processes of Weather.* Cambridge University Press, 445 pp.